EDITOR'S PICK

WILEY **NMR IN BIOMEDICINE**

CO_2 induced pH_i changes in the brain of polar fish: a TauCEST application

Felizitas C. Wermter[1,2] | Bastian Maus[2] | Hans-O. Pörtner[2] | Wolfgang Dreher[1] | Christian Bock[2] 🔟

[1] University of Bremen, Department of Chemistry, in-vivo-MR Group, Bremen, Germany

[2] Alfred Wegener Institute Helmholtz Centre for Polar and Marine Research, Integrative Ecophysiology, Bremerhaven, Germany

Correspondence
Dr Christian Bock, Integrative Ecophysiology, Alfred Wegener Institute Helmholtz Centre for Polar and Marine Research, 27570 Bremerhaven, Germany.
Email: christian.bock@awi.de

Chemical exchange saturation transfer (CEST) from taurine to water (TauCEST) can be used for *in vivo* mapping of taurine concentrations as well as for measurements of relative changes in intracellular pH (pH_i) at temperatures below 37°C. Therefore, TauCEST offers the opportunity to investigate acid–base regulation and neurological disturbances of ectothermic animals living at low temperatures, and in particular to study the impact of ocean acidification (OA) on neurophysiological changes of fish. Here, we report the first *in vivo* application of TauCEST imaging. Thus, the study aimed to investigate the TauCEST effect in a broad range of temperatures (1–37°C) and pH (5.5–8.0), motivated by the high taurine concentration measured in the brains of polar fish. The *in vitro* data show that the TauCEST effect is especially detectable in the low temperature range and strictly monotonic for the relevant pH range (6.8–7.5). To investigate the specificity of TauCEST imaging for the brain of polar cod (*Boreogadus saida*) at 1.5°C simulations were carried out, indicating a taurine contribution of about 65% to the *in vivo* expected CEST effect, if experimental parameters are optimized. *B. saida* was acutely exposed to three different CO_2 concentrations in the sea water (control normocapnia; comparatively moderate hypercapnia OA_m = 3300 µatm; high hypercapnia OA_h = 4900 µatm). TauCEST imaging of the brain showed a significant increase in the TauCEST effect under the different CO_2 concentrations of about 1.5–3% in comparison with control measurements, indicative of changes in pH_i or metabolite concentration. Consecutive recordings of ^1H MR spectra gave no support for a concentration induced change of the *in vivo* observed TauCEST effect. Thus, the *in vivo* application of TauCEST offers the possibility of mapping relative changes in pH_i in the brain of polar cod during exposure to CO_2.

KEYWORDS

chemical exchange saturation transfer (CEST), fish brain, marine ectotherms, pH, taurine (Tau), temperature

1 | INTRODUCTION

Chemical exchange saturation transfer (CEST) was introduced by Ward et al.[1,2] as a signal enhancement technique for MRI, enabling the indirect detection of endogenous or exogenous molecules with exchangeable protons of amide, amine or hydroxyl groups using changes in the NMR signal of the water pool. The intensity of the CEST effect mainly depends on the exchange rates between water and the solute pool, which in turn are influenced by the physical and physiological parameters of the environment such as temperature and pH. Additionally, the concentration of the solute pool impacts the intensity of the effect. These properties allow for CEST to be used for the *in vivo* observation of changes in metabolite concentration in a low millimolar range and in intracellular pH (pH_i).[2]

CEST effects have already been observed and studied *in vitro* for several amino acids such as alanine (Ala), γ-aminobutyric acid (GABA), aspartate (Asp), glutamine (Gln), glutamate (Glu) and taurine (Tau).[3-6] Recent analyses demonstrated the pH (at room temperature)[6] and temperature dependence (at pH 7.0)[5] of the CEST effect between the amine protons of taurine and protons of surrounding bulk water, named TauCEST.

Taurine is an abundant amino acid in the brain of vertebrates, serving as a modulator for neurotransmitter action and an osmoregulator.[7-9] First, the concentration of taurine in the brain depends strongly on the age of the individual. Thus, for rat brain the concentration will decrease from 12mM at birth to 6–8mM in adults.[10] Furthermore, the taurine concentration is species dependent.[11] Because of its osmoregulatory function, taurine is one of the most highly concentrated amino acids in the brains of salt water fish[8] and its concentration depends on the salinity of the seawater.[12] For example, taurine concentrations of up to 65.7mM were found in the brain of stingray (*Dasyatis sabina*),[13] which is one order of magnitude higher than the concentration of around 2mM to 6–8mM in adult rats or humans.[14-17] This makes taurine an ideal candidate for *in vivo* CEST applications to marine organisms.

The current anthropogenic impact on the global climate is also affecting the oceans. Besides ocean warming, anthropogenic CO_2 accumulating in the atmosphere has become enriched in ocean waters and induces so-called ocean acidification (OA), i.e., the changes in sea water carbonate chemistry decreasing water pH due to increasing pCO_2. Ocean surface pH has already decreased by 0.1 units in comparison with pre-industrial times. The additional lowering expected by the end of the 21st century depends on future CO_2 emissions pathways (Representative Concentration Pathways) as projected by the Intergovernmental Panel on Climate Change (IPCC).[18] Thus, ocean surface pH might decrease by 0.4 pH units at the end of 2100 compared with pre-industrial times under unabated emissions.[19]

The most dramatic changes are expected for the polar oceans, inhabited by organisms highly adapted to an energy conserving life at constant low temperatures.[20] Fish have the capability of effective acid–base regulation in their tissues under elevated CO_2 concentrations,[21] which might reduce the threat of OA to this animal group. High ambient CO_2 diffuses across epithelia into the animal, gradually acidifying the extracellular and subsequently the intracellular spaces according to the following formula: $CO_2 + H_2O \leftrightarrow H_2CO_3 \leftrightarrow H^+ + HCO_3^- \leftrightarrow 2H^+ + CO_3^{2-}$. The formation of carbonic acid under elevated CO_2 concentrations is catalysed through carbonic anhydrase in tissues, facilitating an equilibrium of acid and base equivalents (i.e. H^+ and HCO_3^-). Acid–base regulation can then compensate for these ion concentration changes through ion exchange mechanisms. Despite efficient acid–base regulatory capacities, under prolonged exposure to these conditions[21] compensation may be incomplete in some tissues.

Currently, the impact of OA on fish is in the focus of intensive research (for reviews see References 22-25). Thus, various studies have identified CO_2 induced impacts on fish such as olfactory discrimination[26] and the innate ability of fish to detect predator olfactory cues[27] (for a review see Reference 25). These impacts have mostly been studied in tropical and temperate fish species, such as clownfish (*Amphiprion percula*) and damselfish (*Pomacentrus wardi*), providing little information on the effects on polar species, due to their fundamentally different patterns of physiological adaptation.[28,29] Indeed, combined ocean warming and acidification were shown to affect the behavioural laterality of the polar gadid species *Boreogadus saida*.[30]

In previous studies, a connection between a decrease in pH_i and a resulting decrease in the rate of synaptic vesicle release and hence a limited excitability could be shown.[31,32] In this context, changes in the pH_i in the brain in general seem to be indicative of neurological disorders in relation to disturbances in acid–base balance. Therefore, the non-invasive and local determination of the pH_i in the brain of polar fish is desirable to investigate the mechanism underlying neurological and behavioural disorders of fish under OA scenarios.

The determination of pH_i in the tissue of marine organisms can be analysed with high accuracy using the homogenate method established by Pörtner et al.[33] However, the method is invasive, making the time resolved observations of pH_i difficult. *In vivo* ^{31}P NMR spectroscopy is an established non-invasive method for the characterization of high energy phosphates and acid–base regulation in organisms.[34] The pH_i can be determined by the pH dependent chemical shift of intracellular inorganic phosphate, relative to an endogenous reference signal, using an adequate calibration.[35] *In vivo* ^{31}P NMR spectroscopy has already been applied to aquatic animals (for a review see the work of Van der Linden et al.[36]), including polar and marine fish species.[37,38] Nevertheless, the determination of pH_i using ^{31}P NMR spectroscopy has some shortcomings: e.g., the inherently low sensitivity of the ^{31}P nucleus for NMR spectroscopy limits the temporal and spatial resolution. Surface coils are frequently used in ^{31}P NMR spectroscopy, applied close to the tissue, with the shortcoming of an inhomogeneous B_1 field excitation and a limited spatial resolution. The determination of pH_i is therefore restricted to a small range of tissues with a high intrinsic concentration of energy-rich phosphates. CEST imaging seems to be an interesting alternative, offering the possibility to detect pH or metabolites in a low millimolar range, with both high temporal and high spatial resolution.

Owing to its pH and temperature dependence as well as the high concentration of about 20mM in the brain of polar fish, the CEST effect of taurine is a promising tool for detecting pH_i changes in the brain of polar fish to improve the understanding of mechanisms underlying the

observed neurological changes. For the application of TauCEST on polar fish, the aim of this study is to investigate the TauCEST effect under different CO_2 concentrations and at low temperatures. Additionally, the specificity of the TauCEST effect and the contributions of other amino acids to the total CEST effect observed *in vivo*, as well as the optimal experimental parameters, are examined. Finally, the feasibility of applying TauCEST to the brain of polar cod under comparatively moderate and high CO_2 levels is demonstrated for the first time.

2 | MATERIAL AND METHODS

2.1 | *In vitro* phantom studies

The *in vitro* NMR measurements were made on a 7 T animal scanner (BioSpec 70/20 USR, Bruker BioSpin, Ettlingen, Germany) equipped with a BGA-12S2 B_0 gradient system and using ParaVision 5.1. RF excitations and signal detection were achieved with a quadrature birdcage coil with an inner diameter of 72 mm. FASTMAP (Fast Automatic Shimming Technique by Mapping Along Projections) was used to optimize B_0 homogeneity, ensuring line widths of 8 Hz or less.[39]

CEST imaging was conducted with a pre-saturated single-slice FISP (fast imaging with steady-state precession) sequence using centred phase encoding and the following sequence parameters: field of view (FOV) 35×35 mm^2, matrix size 64×64, slice thickness 2 mm, flip angle 9°, delay between signal excitation within the FISP imaging sequence $T_{R1} = 3.2$ ms and echo time $T_E = 1.6$ ms.[5] Pre-saturation was accomplished by a train of 12 rectangular pulses with an RF irradiation amplitude $B_1 = 5.87$ μT, pulse width 1 s and an interpulse delay of 50 μs. Z-spectra were obtained at 31 frequency offsets $\Delta v = \Delta\omega/2\pi$ between −1500 and 1500 Hz in steps of 100 Hz. After acquiring each FISP image, the residual z-magnetization was destroyed by a 90° sech pulse. The repetition time of the complete CEST imaging sequence was $T_{R2} = 15$ s.

The signal minimum in the z-spectrum at the water signal was fitted to a Lorentzian lineshape to correct for B_0 inhomogeneities.[40] Z-spectra were obtained by plotting the normalized signal intensity as a function of frequency offset ($\Delta\omega$ [ppm]). The CEST asymmetry was calculated as

$$CEST_{asym} = \frac{M_{sat}(-\Delta\omega) - M_{sat}(\Delta\omega)}{M_{sat}(-\Delta\omega)}$$

where M_{sat} refers to the magnetization with saturation at a positive ($\Delta\omega$) or a negative ($-\Delta\omega$) offset from the water resonance.[5]

The impact of pH and temperature on TauCEST z-spectra and asymmetry curves were studied on a phantom, consisting of six NMR tubes filled with 10mM taurine, dissolved in phosphate buffered saline (12mM HPO_4^{2-}, 0.1 M NaCl). Solutions of different pH values of 5.5, 6.0, 6.5, 7.0, 7.5 and 8.0 were used in an agarose phantom wrapped with temperature controlled heating tubes for measurements at defined temperatures (1–37°C, accuracy: ±0.1°C).[5] The chemical shift between the amine protons of Tau and the water resonance was assumed to be 2.8 ppm.[6,41] All phantom experiments were repeated five times. The results are expressed as a mean ± standard deviation.

2.2 | Simulations

Simulations were performed by numerically solving the Bloch-McConnell equations using a two-pool model or a multi-pool model[5,42] for 9.4 T. The metabolites used were GABA (2.8mM), Gln (2.8mM), Glu (5mM) and Tau (20mM), which are the most prominent amino acids with exchangeable protons in the polar cod brain.[43] The total Cr (tCr) concentration, i.e. sum of creatine (Cr) and phosphocreatine (PCr), was assumed to be 7mM, which is a reliable concentration for a polar cod brain. This concentration was used to derive absolute values of the other metabolites, because Schmidt et al. published only relative concentrations using tCr as reference.[43]

The simulations used exchange rates experimentally determined by fitting the Bloch-McConnell equations, modified for a two-pool chemical exchange, to the experimental data. The calculated exchange rates for the different metabolites are shown in Table S1 of the supplementary material. The relaxation times for water were obtained from *in vivo* measurements on polar cod brain, $T_{1a} = 1.15$ s and $T_{2a} = 45$ ms (data not shown). The relaxation times of the exchangeable protons of the amino acids, which are, however, inconsequential for the simulations, were fixed to $T_{1b} = 1$ s and $T_{2b} = 10$ ms.[44,45]

2.3 | *In vivo* fish studies

2.3.1 | Experimental setup and protocol

Polar cod *B. saida* were provided by the University of Tromsø, Norway. In January 2013, polar cod were caught from the R/V Helmer Hanssen with a bottom trawl in a depth of 120 m in Kongsfjorden (78° 97′ N 12° 51′ E) at the western coast of Svalbard. From late April 2013, the individuals were kept in sea water aquaria at 1.5°C at the Alfred Wegener Institute in Bremerhaven. Fish were fed once a week with frozen cockles.

In vivo MR measurements were made in a 9.4 T animal scanner with a 30 cm bore (BioSpec 94/30 USR, AVANCE III, Bruker BioSpin, Ettlingen, Germany) equipped with a BGA-12S HP B_0 gradient system and running under ParaVision 6.0.1. A quadrature birdcage coil (86 mm inner diameter) was used for RF excitation and signal detection.

Prior to the MRI measurements, the fish was placed in a Perspex flow-through chamber ($V = 350$ ml; Figure 1). The chamber was lined with dental wax to align to the shape of the individual fish. In this way, the unanaesthetized fish stayed positioned in front of the water inflow but was
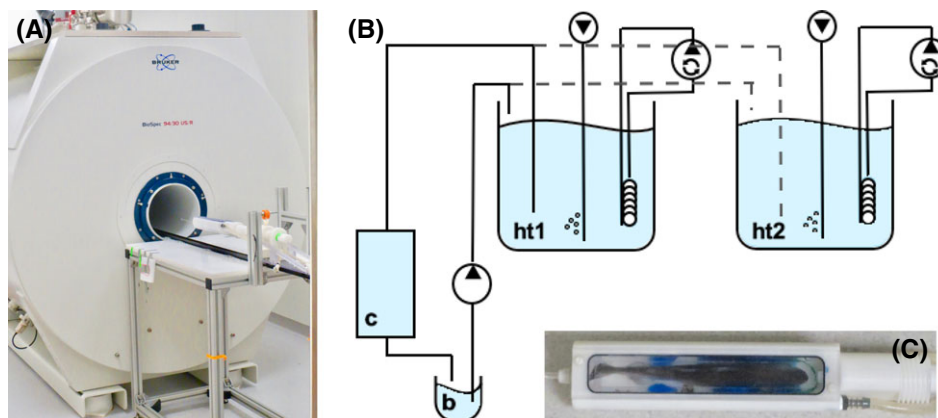
FIGURE 1 A, 9.4 T animal scanner (BioSpec 94/30 USR, Bruker BioSpin) equipped with the positioning aid and the flow-through chamber. B, Scheme of experimental setup with a sea water circulating system consisting of two header tanks (ht1 and ht2) and the flow-through chamber (c) and a bin (b). C, Recirculated flow-through chamber including an unanaesthetized polar cod sitting in front of the water inflow

still able to use its fins. The chamber was connected to an in-house developed positioning aid and placed with the head of the fish in the centre of the magnet (see Figure 1A). A constant water flow through the chamber (about 500 ml/min) was maintained by hydrostatic pressure and supplied by temperature controlled sea water reservoirs (50 l each) similar to the setup in Reference 37. The water temperature in the chamber was maintained at 1.5°C by circulation thermostats in the reservoir, confirmed by temperature measurements with a fibre-optic thermometer (OPTOCON AG, Optical Sensors and Systems, Dresden, Germany) in the reservoirs and behind the outflow of the chamber inside the magnet.

Two sea water reservoirs were used: (i) at control conditions bubbled with air; and (ii) at elevated CO_2 bubbled with an air/CO_2 mixture from a gas-mixing pump (PR 4000, MKS Instruments, Munich, Germany), simulating comparatively moderate (OA_m) and high (OA_h) CO_2 conditions. A summary of water chemistry is given in Table 1.

The stability of the condition was verified by measuring the pCO_2 before and after the experiments. The pH and salinity were monitored subsequent to the experiments. Water pCO_2 was determined from the gas phase of the sea water by a combined carbon dioxide probe (CARBOCAP GMP343, Vaisala, Helsinki, Finland) and carbon dioxide meter (CARBOCAP GM70, Vaisala). For pH measurements, a pH meter (pH 3310, WTW, Weilheim, Germany), which was calibrated with thermally equilibrated NBS buffer (two-point calibration), was used. The pH values were cross-calibrated to total pH scale using Tris-buffered pH reference material (Batch 4, Marine Physical Laboratory, University of California, San Diego, CA, USA). Temperature and salinity were measured using a WTW LF 197 multimeter (WTW).

The experimental protocol was as follows:

Day 1. Acclimation of the fish to the new environment inside the scanner under control conditions using header tank 1 (ht1) for at least 18 h.

Day 2. CEST and localized ^1H NMR measurements at control conditions (2 h at least), followed by a switch to the first OA scenario (OA_m (n = 3) or OA_h (n = 2)) using header tank 2 (ht2). Again, CEST measurements were recorded consecutively for 4 h and an ensuing reconnection to the control conditions was established for at least 18 h. After 1.5 h of exposure to elevated CO_2, localized ^1H NMR measurements were repeated.

Day 3. The same procedure as for Day 2, but switched to the second OA scenario (OA_m (n = 2) or OA_h (n = 3)). After a final period under control conditions for at least 1.5 h, the experiments were finished. OA scenarios were chosen randomly to exclude acclimation or training effects. All animals contributing to the data set survived the normal experimental procedure and were transported back to the aquarium (n = 5).

2.3.2 | NMR methods

Fast overview image scans of three perpendicular slices (tri-pilot) were used to position the head of the animal. Additionally, B_0 homogeneity was improved for the whole head volume of the fish using a MAPSHIM protocol, which exploits a 3D map of the B_0 field and calculates the optimal shim values.

TABLE 1 Water chemistry of all treatments

Treatment	Control	OA_m	OA_h
pH (free scale)	8.04	7.18	7.00
HCO_3^- [μmol/kg SW]	2818	2355	2332
pCO_2 [μatm]	540	3300	4900
Temperature [°C]	1.5	1.5	1.5
Salinity [psu]	32.8	32.8	32.8

For anatomical studies as well as slice and voxel selection, multi-slice RARE imaging was performed in coronal, sagittal and axial directions, with the following sequence parameters: FOV 50 × 50 mm^2, matrix size 256 × 256, 10–20 slices, slice thickness 1 mm, slice gap 0 mm, in-plane resolution 0.195 mm, T_R = 4000 ms, T_E = 51.88 ms, RARE factor 8, scan time 8 min 32 s for four averages.

Localized ^{1}H NMR spectra were acquired for studying potential changes in metabolite concentration throughout the experimental protocol. A standard localized ^{1}H point resolved spectroscopy (PRESS) sequence[46] was used. The sequence parameters were as follows: voxel size 3.5 × 5 × 3 mm^3, T_E = 16.3 ms, T_R = 2500 ms, spectral width SW = 4401 Hz, 2 k complex data points measured, scan time 10 min 40 s for 256 averages. Additionally, an eddy current compensation was performed using the unsuppressed water signal. The PRESS sequence was preceded by seven RF pulses with variable pulse power and optimized relaxation delays (VAPOR) used for water suppression.[47] Outer volume suppression was realized by the suppression of four slices around the voxel with a thickness of 5 mm.

CEST imaging was similar to the *in vitro* studies. The sequence parameters were as follows: FOV 48 × 48 mm^2, matrix size 128 × 64, slice thickness 4 mm, flip angle 9°, T_{R1} = 3.0 ms, T_{R2} = 16 s, T_E = 1.65 ms. Pre-saturation was accomplished by a train of three rectangular pulses with an RF irradiation amplitude B_1 = 4.4 μT, pulse width 1 s and interpulse delay 50 μs (saturation time (*t*) ~ 3 s). Z-spectra were obtained using 50 frequency offsets $\Delta \nu = \Delta \omega / 2\pi$ between −20 000 and 20 000 Hz with respect to the water signal (−20 000, −10 000, −5000, −2250, −2125, −2000, −1875, −1750, −1625, −1500, −1375, −1250, −1125, −1000, −875, −750, −625, −500, −375, −250, −188, −125, −62, 0, 62, 125, 188, 250, 375, 500, 625, 750, 875, 1000, 1125, 1250, 1375, 1500, 1625, 1750, 1875, 2000, 2125, 2250, 5000, 10 000 and 20 000, all in Hz). For normalization, fully relaxed images were acquired with a large off-resonance frequency of the saturation pulse (−100 kHz).

2.3.3 | Data evaluation and statistics

The analysis of the CEST images was identical to that for the *in vitro* studies. The data points shown for controls (Control I and Control II) were recorded immediately before switching to the OA conditions and correspond to the mean value of four data points for each fish. The data obtained under OA conditions were recorded after 1.5 h, again calculating the mean value of four data points for each fish. The effects for all conditions were illustrated in relation to the mean of the first control measurements of each fish. Normal distribution of each group was investigated by the Shapiro–Wilk test, yielding P = 0.896. Therefore, different treatments were tested for significance using a one-way ANOVA for repeated measurements with a Student–Newman–Keuls multiple comparison test ($p < 0.05$). Statistical outliers were identified using a Nalimov test (α = 0.05).

3 | RESULTS

3.1 | *In vitro* MR phantom studies

Figure 2 shows *z*-spectra of 10mM taurine solutions (circles) and the corresponding asymmetry curves at different pH values (5.5–8.0) measured for a temperature range from 1 to 37°C. A chemical shift difference of 2.8 ppm between water and the exchanging protons of taurine was assumed, thus neglecting the shift of water resonance due to a change in temperature.[5] The direct saturation is comparable for the whole pH and temperature range. Figure 2A depicts *z*-spectra and asymmetry curves for 37°C and different pH values. A considerable CEST effect is only visible at a pH lower than 6.5. Above pH values of 6.5, a TauCEST effect cannot be detected at 37°C. However, with decreasing temperatures, the asymmetry curves increase for pH values of physiological interest (see, e.g., pH 7.0 at 25°C and pH 7.5 at 15°C, Figure 2C-E).
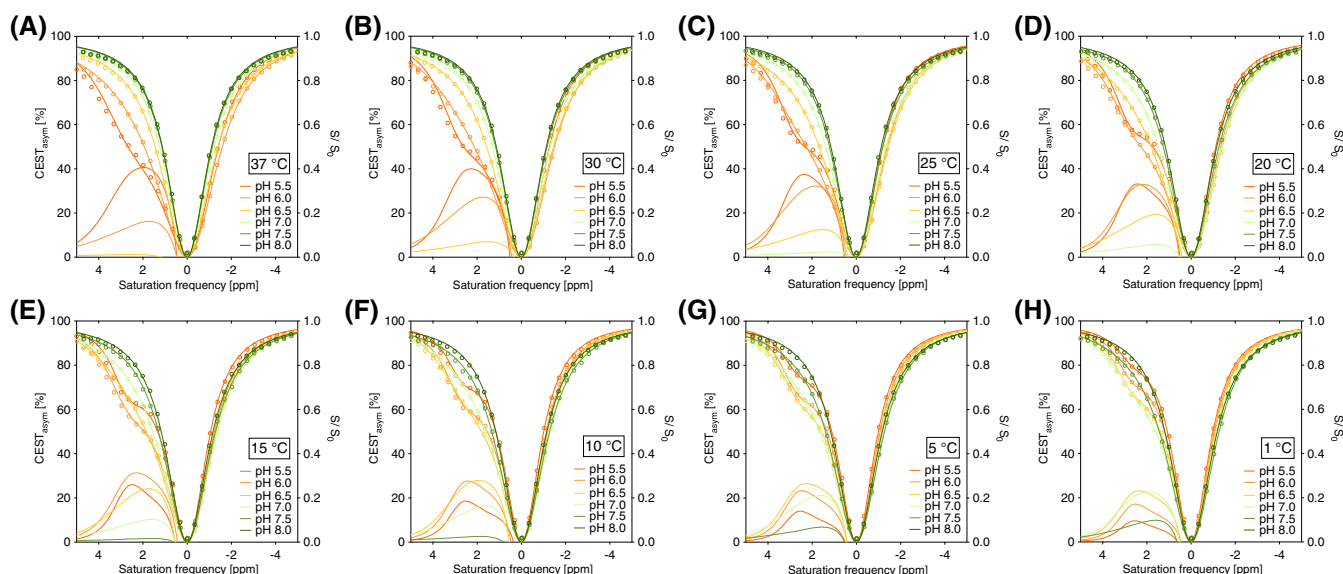

FIGURE 2 Dependence of TauCEST on pH and temperature at 7 T. Experimentally determined TauCEST *z*-spectra (circles) and corresponding asymmetry curves were measured on 10mM taurine solutions at different pH values (5.5–8.0) and temperatures (1–37°C) (B_1 = 5.87 μT)

The asymmetry curves at 1°C show a clear dip for the pH range of 5.5–7.5, even if the TauCEST effect is not a strictly monotonic function of pH (Figure 2H and Figure 3A). For the experimental saturation parameters used, TauCEST increased gradually from pH 5.5 to pH 6.5 and then sharply decreased from pH 6.5 to pH 7.5. Thus, the TauCEST effect changes monotonically in the physiological range of interest (pH 6.8–7.5) at 1°C.

The TauCEST effect depends on the taurine concentration and increases at pH 7 and 1°C with increasing concentration (Figure 3B, C). Additionally, the effect also depends on B_1 amplitude, indicating that it is possible to obtain higher TauCEST effects at higher B_1 (Figure 3C).

Figure 4 displays the results from a simulation of asymmetry curves at 2.8 ppm as a function of B_1 and pH for the amino acids GABA, Gln, Glu and Tau at 1.5°C (B_0 = 9.4 T). The effect was simulated for the individual amino acids with a two-pool model, while the common effect of all amino acids was simulated with a multi-pool model. The asymmetry curves indicate a maximum intensity for the total CEST effect of all amine protons at 7.1 µT, whereas the pure TauCEST effect shows its highest intensity between 8.3 and 9.9 µT (pH 7.3) (Figure 4A). The CEST effects of the other metabolites, i.e. GABA, Gln and Glu, exhibit their maxima at lower B_1 (<4 µT). However, we used a B_1 = 4.4 µT as a compromise between intensity and specificity of the CEST effect and the magnetization transfer effect expected in vivo. Additionally, we wanted to avoid any SAR problems by using long continuous wave preirradiation with high B_1. The CEST asymmetry curves were also simulated as a function of pH and for a B_1 of 4.4 µT (Figure 4B). Additionally, the percentage contributions of each amino acid to the added two-pool simulations were determined (Figure 4C). Whereas both the total CEST effect of all amine protons and the pure TauCEST effect are strongest at pH 6.5 and decrease with increasing pH, the effects of GABA and Glu increase with increasing pH. For this reason, even the specificity of the CEST effect of the amino acids changes as a function of pH (Figure 4C). Taurine dominates the total CEST effect for a pH between 6.5 and 7.5, but the percentage contribution decreases from 75% to 40% with increasing pH. However, the TauCEST effect shows the same course as the total CEST effect of the multi-pool model, despite of the dominating effect of Glu between pH 7.6 and 8.0.

3.2 | *In vivo* MR studies on fish brain

The interpretation of the anatomical images for *B. saida* (Figure 5) and the assignment to the different brain regions is based on the work of Eastman and Lannoo.[48] The anatomical images allow for a clear distinction between the brain and the surrounding tissue as well as for the
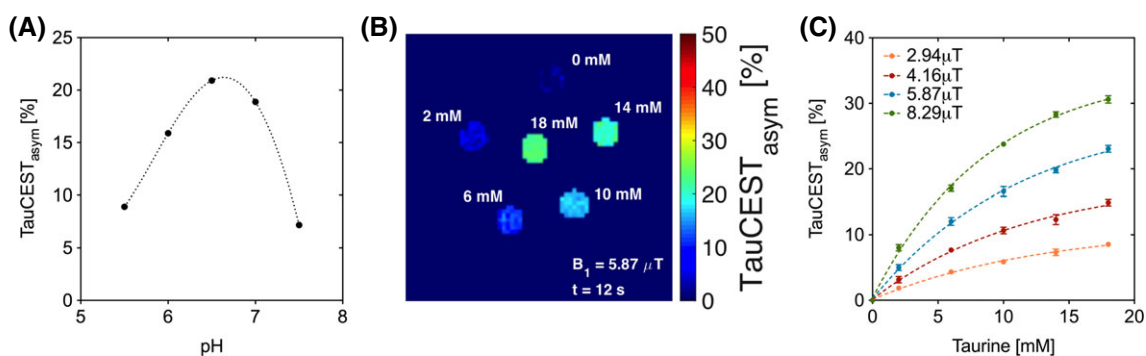

FIGURE 3 TauCEST: pH and concentration dependence at 7 T. A, Dependence of TauCEST on pH from 5.5 to 7.5 for 1°C, showing a monotonic decline of the CEST effect between pH values of 6.8 and 7.5 (10mM, B_1 = 5.87 µT) (the dotted line represents a fit with a fourth degree polynomial as visual aid). B, C, TauCEST asymmetry images measured on a phantom with different taurine concentrations (pH 7.0, B_1 = 5.87 µT, t = 12 s, T = 5.5°C) and dependence of the TauCEST effect on taurine concentration [mM] for different B_1 [µT] (7.0 pH, t = 12 s, T = 5.5°C), indicating a higher TauCEST effect with increasing Tau concentrations and B_1 (dotted lines represent the fit of a one-phase association)
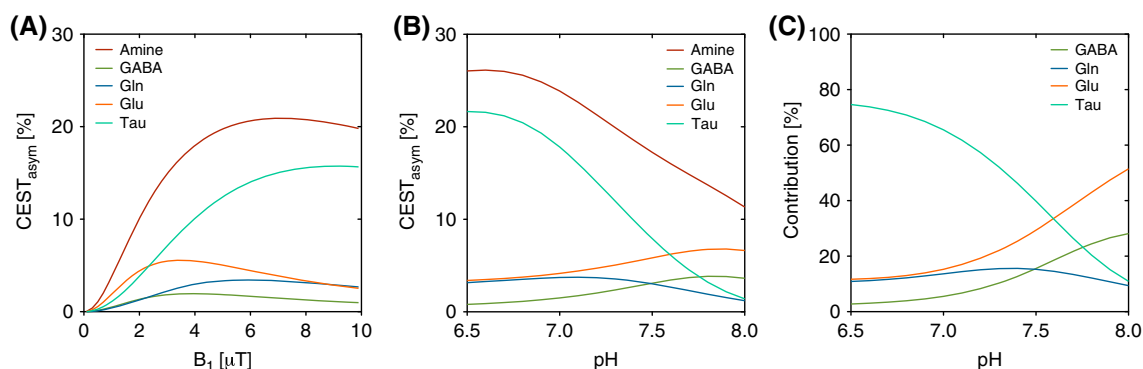

FIGURE 4 A, B, Two- and multi-pool simulations of asymmetry curves at 2.8 ppm as a function of B_1 (pH 7.3) and as a function of pH (B_0 = 9.4 T; B_1 = 4.4 µT) for polar cod brain at 1.5°C. C, The percentage contributions from the added two-pool simulations to the total CEST effect. Taurine shows the highest contribution to the total CEST effect at pH 6.5–7.5
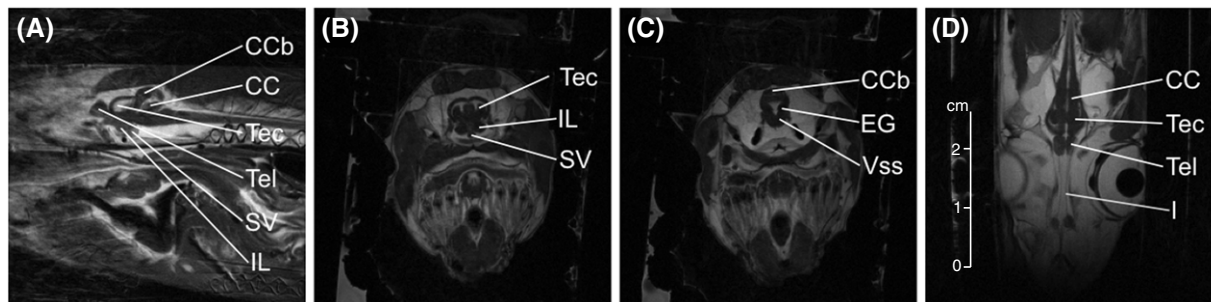
FIGURE 5 *In vivo* morphological brain MR images of *B. saida* acquired at 9.4 T. The slices show sagittal A, axial B, C and coronal D images of the head: CCb, corpus division of the cerebellum; EG, eminentia granularis division of the cerebellum; I, olfactory nerve; IL, inferior lobe of the diencephalon; SV, saccus vasculosus; VSS, spinal sensory nucleus of the trigeminal nerve

identification of major brain regions, i.e. the crista cerebellaris of the rhombencephalon (CC), the tectum of the mesencephalon (Tec) and the telencephalon (Tel). Additionally, refined details such as the olfactory nerve (Figure 5D) can be identified.

Figure 6 shows results of the *in vivo* TauCEST studies performed on polar cod under different CO_2 conditions. The CEST asymmetry curves were obtained from region of interest positions in the CC of the brain (see Figure 6A). The asymmetry curves are rather broad and show sharp maxima at around 1 ppm. However, a clear difference between the two treatments in comparison with control could be identified at about 2.8 ppm, which can be attributed to TauCEST. Thus, the TauCEST effect increases from around 9% for the control measurements to about 11% in this example for the OA_h scenario. Similar results were observed in all five individuals.

In Figure 6C the TauCEST effects for all conditions are displayed in relation to the mean of the first control measurements of each fish to account for potential inter-individual variations in taurine concentration. The Control II measurement for Fish 2 was identified as an outlier (Figure 6C, green framed dot). Therefore, the control measurements before and after the first CO_2 treatment show no significant differences (−0.02 ± 0.42% (without outlier)). The OA_m treatment shows a significant increase in the TauCEST effect after 1.5 h of exposure (1.34 ± 0.40%) in comparison with Control I ($p = 0.007$). At the OA_h scenario the TauCEST effect increased significantly by 3.17 ± 1.04% after 1.5 h of exposure (Control I versus OA_h, $p = 0.005$; OA_m versus OA_h, $p = 0.029$). Figure 6D shows an example of localized ^1H MR spectra (located
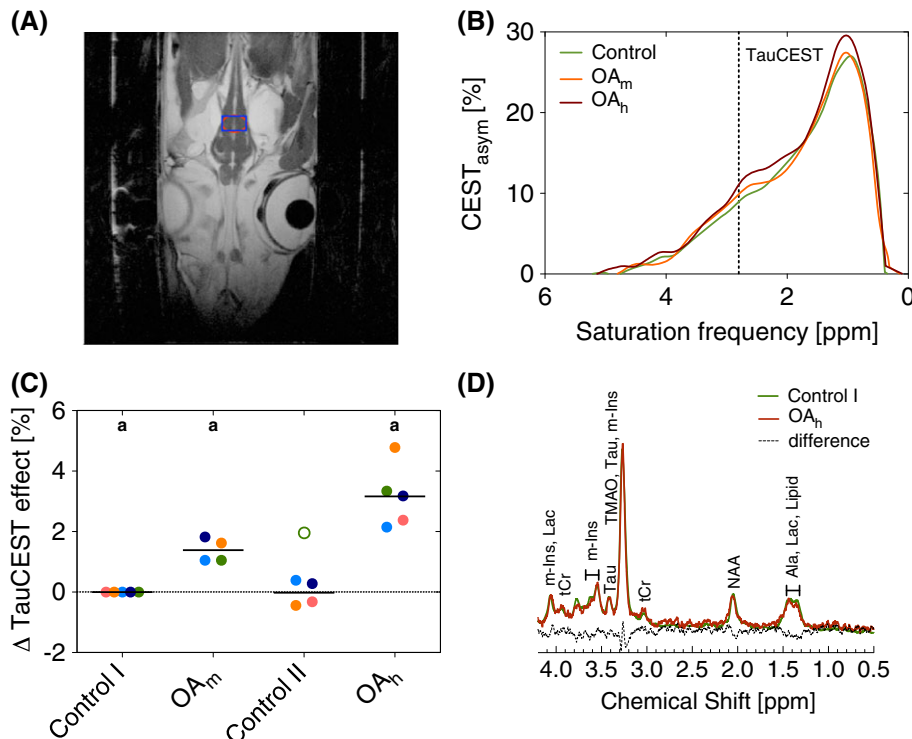

FIGURE 6 MRI and ^1H MRS data from the brain of a polar cod *B. saida* acquired at 9.4 T. A, Anatomical image of a coronal slice with the region of interest (red line), which was used for the CEST analysis of the head region of polar cod and the corresponding voxel (blue line) used for localized ^1H MRS. B, Example of *in vivo* asymmetry curves and the expected TauCEST effect at 2.8 ppm (dotted line) during the first control phase (green) as well as under OA_m (3300 µatm, orange) and OA_h conditions (4900 µatm, red). C, Changes in the TauCEST effect after 1.5 h under hypercapnia with respect to the mean of the first control measurements of each animal (light blue dots, Fish 1; green dots, Fish 2; pink dots, Fish 3; light blue dots, Fish 4; orange dots, Fish 5). D, ^1H MRS spectra obtained from the brain of the polar cod under control conditions (green) and at the end of OA_h (red)

in the same region as for the CEST measurements), which were obtained directly after the experimental protocol of the OA_h treatment, in comparison with a ^1H MR spectrum acquired during the first control phase to demonstrate that the *in vivo* TauCEST effect is predominantly related to changes in pH and not in taurine concentration (Figure 6D). The main resonance line is the methyl signal (at 3.28 ppm) of trimethylamine oxide (TMAO), a prominent amine oxide osmolyte usually found in marine fish. In addition, signals of typical brain metabolites such as N-acetylaspartate (NAA), Ala, tCr, myo-inositol (m-Ins) and Tau can be clearly identified in the ^1H NMR spectra (cf. Figure 6D).

4 | DISCUSSION

The dependence of the CEST effect between the amine protons of taurine and protons of bulk water on pH and temperature has already been shown *in vitro*,[5,6] while a proof of concept for TauCEST *in vivo* has been missing. In particular, the application of TauCEST for pH_i measurements has not been shown before. Against this background, the aim of this study was to systematically examine the *in vitro* TauCEST effect over a wide range of pH, taurine concentration and temperature. Additionally, the specificity of TauCEST was investigated in order to adapt this technique for *in vivo* applications on ectothermic animals at temperatures below 37°C. As a first application, the impact of high CO_2 concentrations on the acid–base regulation of the brain of the polar cod *B. saida* was shown.

4.1 | *In vitro* observations and simulations

The *in vitro* studies showed the expected dependence of the TauCEST effect on pH and temperature, which is determined by the exchange rates between the amine protons of taurine and the protons of bulk water. The observed proton exchange is dominated by a base catalysed exchange, so it depends on the concentration of the OH^- ions in the solution. An increase in pH results in an exponential increase of the exchange rate.[49,50] Additionally, the exchange slows down with decreasing temperature, as defined by the Arrhenius equation.[51] For TauCEST imaging performed with the applied experimental parameters, these properties ensure that the intermediate-exchange regime, defined as $\frac{k_{sw}}{\Delta\omega}\sim 1$, will be reached at low temperatures and the physiological pH range (Figure 2E-H).[1]

However, the intensity of the TauCEST effect as a function of pH is not strictly monotonic for most of the temperatures (Figure 2), due to varying exchange rates. Thus, the optimal labelling efficiency (α), which yields a measure of the maximal CEST effect, depends on both the exchange rate (k_{sw}) and the applied B_1: $\alpha = \frac{(\gamma B_1)^2}{(\gamma B_1)^2 + k_{sw}(k_{sw} + R_{2b})}$.[52] However, as shown for a temperature of 1.5°C, an unambiguous relation between the intensity of the TauCEST effect and the pH value can be obtained for the pH range of interest (pH 6.8–7.5) with the experimental parameters used (Figure 3A).

Besides taurine, a number of other amino acids and brain metabolites show CEST effects in the specific spectral region of 2.8 ppm, which can change with concentration and temperature. Therefore, simulations were carried out to obtain optimal experimental parameters for the detection of TauCEST and to determine the specificity as a function of pH. Thus, a mixture of metabolites was analysed for 1.5°C, mimicking the intracellular composition of a polar cod brain. Intracellular concentrations of main metabolites were determined from a previous study on OA effects on neurophysiological changes in polar cod.[43] In particular, the metabolites GABA, Gln, Glu and Tau, which were found with significant concentrations and exhibit exchangeable protons around 3.0 ppm from water, were used for the *in vitro* studies. Other prominent brain metabolites such as Cr and m-Ins were neglected, since the CEST effects of these compounds did not significantly overlap with the TauCEST region (-OH of m-Ins 0.6 ppm and $(NH_2)^+_2$ of Cr 1.9 ppm from water[53,54]). In addition, the exchangeable protons of NAA were not taken into account, because the very slow exchange rate[55] prevents the detection of a CEST effect of NAA at low temperatures.[5]

The simulations indicate that a compromise between the signal-to-noise ratio and the specificity of TauCEST is required (Figure 4A). To achieve a maximal sensitivity of the TauCEST effect and a taurine contribution of more than 50% to the CEST effect, a B_1 amplitude of 4.4 μT was chosen for the subsequent simulations and the *in vivo* measurements. According to this, the contribution of taurine will be 65% of the expected effect in the physiological pH range *in vivo* with contributions of about 35% from other brain metabolites with exchangeable protons (Figure 4C). This is in the same range as the expected contribution of Glu to the *in vivo* GluCEST (CEST from Glu to water) effect measured in the human brain at 37°C of 70–75%,[3] thus justifying the term TauCEST. Additionally, the TauCEST effect shows a similar pH dependence to the total CEST effect in the multi-pool simulation, i.e. decreasing intensity with higher pH. This is of central importance, since the characteristics of the multi-pool are crucial for the usefulness of CEST imaging.[3,6] Therefore, the *in vitro* measurements and the simulations predict the applicability of TauCEST for *in vivo* studies on polar cod at low temperatures and its use for detecting relative changes in pH_i.

4.2 | *In vivo* studies

In contrast to the *in vitro* measurements the *in vivo* studies were carried out on a 9.4 T animal scanner specially dedicated for marine organisms. Since the simulations are based on the determination of field independent exchange rates, the CEST method can be easily adapted for higher field strengths.

The high resolution of the anatomical images allows us to distinguish different brain regions of an unanaesthetized and ventilating fish at 9.4 T. In spite of the small volume of the polar cod brain in comparison with conventional animal models such as rat (rat brain ~13 mm × 13 mm × 8 mm,[56] polar cod brain ~15 mm × 6 mm × 5 mm (this study)) (see Figure 5), different brain areas such as cerebellum, diencephalon and olfactory nerve can be identified in the MRIs, which could not be achieved in unanaesthetized and versatile fish previously; see, e.g., Reference 37. In a previous study, anatomical images of an anaesthetized and restrained freshwater zebrafish (*Danio rerio*) in a vertical bore system were acquired (FOV 1 cm, matrix 256 × 256, slice thickness 0.2 mm).[57] However, this is the first time that anatomical images with such a high resolution of an unanaesthetized fish *in vivo* have been shown. The images indicate no movement artefacts, despite the nearby movement of the gills for ventilation (located below the brain; see Figure 5B, C), which is a prerequisite factor for further data evaluation. In addition, the high quality and repeatability ensure that the same region of interest could be used for analysing the CEST effect in the same brain area during the entire experiment and for all individuals studied (see Figure S2 of the supplementary material).

The course of the *in vivo* asymmetry curves was comparable for all treatments and individuals, showing a clear TauCEST dip at about 2.8 ppm, which increases with increasing CO_2 concentration (Figure 6B), although the maximum of the asymmetry curve that occurs around 1 ppm was somewhat surprising. It is intriguing that the maximum at 1 ppm showed also an increase with elevated CO_2 concentrations. The background of this incidental finding and the clear identification of the source of the CEST effect at 1 ppm needs further studies.

The analysed TauCEST effects for all conditions were calculated in relation to the mean of the first control measurements (Figure 6C). Therefore, relative changes in the TauCEST effect are still comparable, even if, for instance, the taurine concentrations varied between the individuals. The standard deviations between the individuals are small for both controls and the OA_m group. The OA_h group showed higher variations, most likely caused by increased movement, possibly due to enhanced gill ventilation of fish under hypercapnia.[58] Furthermore, it can be concluded that the *in vivo* observed TauCEST effects result from the physical and physiological parameters of the intracellular space, because of the two magnitudes higher intracellular taurine concentration in comparison with the extracellular concentration.[59]

A significant increase in TauCEST effects for the moderate and high CO_2 treatment of about 1.5% and 3%, respectively, was observed in all animals, indicating either an increase in intracellular Tau concentration or a decrease in pH_i (Figure 6C). Simulations predict that the observed changes in the TauCEST effect of about 1.5% and 3% would require an increase of about 7 and 14mM in Tau concentration or a decrease by about 0.2 and 0.4 pH units, respectively. Modifications in the T_1 of water and B_1 can be ruled out. Simulations show that a change in the water T_1 by 100 ms will result in a change of about 0.75% of the total CEST effect. Therefore, it is unlikely that T_1 changes are the major cause of the observed increase in the total CEST effect by 3%. This is particularly true as temperature induced changes in T_1 can be excluded due to a continuously measured and controlled temperature of the water reservoirs via a feedback controlled thermostat. In addition, the B_1 amplitude was readjusted prior to every new experimental condition to avoid such unwanted changes. A change in the B_1 of 4.4 μT by 0.1 μT would result in a change of about 0.18% of the total CEST effect. However, a larger decrease in B_1 would reduce the expected total CEST effect, while a larger increase would not lead to a considerable increase in the CEST effect because the CEST asymmetry curve is already close to the broad maximum (cf. Figure 4A).

In order to investigate the cause of the *in vivo* observed increase in TauCEST with increasing CO_2 concentrations, localized ^{1}H MR spectra were acquired in the brain of polar cod in the same region as for the analysis of the CEST effect (Figure 6D). In previous studies, localized ^{1}H MR spectra were recorded in the brain of an anaesthetized zebrafish (*Danio rerio*).[57] Our spectra are comparable but recorded in unanaesthetized fish. Anaesthesia may impact brain metabolism, e.g. through effects on inhibitory and excitatory postsynaptic receptors[60] and acid–base balance.[61] The spectra enable a very good separation of various important brain metabolites, i.e. NAA, Cr, m-Ins and Tau. Since the spectra were acquired at different time points, they differ in shim quality and line width. In order to ensure comparability, differences in sensitivity were corrected using the unsuppressed water signal and the data sets were processed with an adapted apodization aiming at similar linewidths in the phase corrected spectra. However, a visual inspection of the localized ^{1}H MR spectra acquired at the end of the first control phase and after OA_h treatment supported by a difference spectrum showed no increase in Tau concentration. Therefore, an increase in Tau concentration can be excluded as an explanation for the observed increase in the CEST effect at 2.8 ppm. An increasing concentration of other amino acids contributing to the *in vivo* expected CEST effect by about 1mM would result in an increase of the CEST effect by 0.5%. However, the only difference that was observed during CO_2 incubation was a decrease in Glx signal intensity for the OA_h treatment. This is in agreement with a previous *in vitro* study, which found a decrease in Glu concentration in the brain of polar cod after 100 days of exposure to OA, albeit using lower pCO_2 and slightly lower temperatures (0°C, pCO_2 ~1000 ppm).[43] However, a decrease in metabolite concentration would result in a corresponding decrease in CEST effect.

According to these arguments, it can be concluded that the observed increase in the TauCEST effect under elevated pCO_2 is a result of decreasing pH_i in the brain of polar cod *B. saida*. This indicates a slowed pH compensation in polar cod despite the good capacity for acid–base regulation in fish. A decrease in extra- and intracellular pH under mild hypercapnia is visible mostly in lower invertebrates under acute exposure to mild elevations in pCO_2,[62] whereas fish usually display full compensation. In Atlantic cod (*Gadus morhua*), a transient decrease in pH_i of about 0.07 and 0.25 pH units was observed in muscle and liver tissue, respectively, during exposure to an extremely high CO_2 concentration of 10 000 μatm at 12°C.[63]

The buffering capacity of the intracellular space is determined by (passive) non-bicarbonate buffers, also including inorganic and organic phosphates, and varies between species and tissues.[21] In addition to passive buffering capacities, active processes contribute to pH_i regulation, such as the Na/K-ATPase and the V-type H^+ ATPase (driving the exchange of Na^+ and H^+). Active acid–base regulation may be visible in the comparable control groups: The pH_i therein is elevated to control values after both OA challenges, indicated by a decrease of the CEST effect for nearly all

individuals (Figure 6C). However, the TauCEST effect for Fish 2 still increased after the first high CO_2 exposure, which might indicate an insufficient capacity of acid–base regulation in fish over 18 h.

In comparison to the OA scenarios as predicted by the IPCC, the CO_2 concentrations used in this study are too high to support a realistic projection at ecosystem level. However, future studies will be able to detect even smaller changes in pH_i with a high spatial and temporal resolution using TauCEST. Therefore, our study provides the first evidence for in vivo TauCEST imaging to detect changes in pH_i at a high spatial and temporal resolution in polar and marine organisms (see also Figure S2 of the supplementary material). This is highly beneficial compared with ^{31}P NMR spectroscopy, which displays low resolution due to low sensitivity and a localization usually dependent on the diameter of the surface coil. In previous studies localized ^{31}P MR spectra with an excellent spectral resolution and small voxels (27–45 mm^3) were obtained in mouse brain.[64,65] Nevertheless, the time resolution for the acquisition of such spectra is usually around 30 min or longer, and the applicability of localized ^{31}P NMR spectroscopy in a sea water environment still needs to be demonstrated.

Using polar cod as an experimental animal, and focusing on TauCEST instead of the more widely used GluCEST,[3,5,66-68] it has been shown that CEST effects are far from being limited to a previously established application. Absolute pH_i measurements in vivo are not yet possible, even if the dependence of k_{sw} on pH and T is clearly determined, since the influence of varying molecular environments in living tissue with differing pH buffer systems and solutes is not fully disclosed.[51] In the next phase of this project, the influence of magnetization transfer between water and protons of varied macromolecules on the in vivo TauCEST effect should be investigated,[69,70] to establish absolute pH_i mapping. However, relative pH_i changes can be monitored. In future studies, the TauCEST effect should be further improved by optimizing the list of used frequency offsets, i.e. centred detection around the direct saturation (~0 ppm) and about 2.8 ppm with respect to the water frequency. This will shorten the measurement time per data set, thus further reducing movement artefacts. Future studies also should investigate long-term responses to elevated CO_2, in combination with an accurate analysis of pH_i over time to clarify the time course of pH_i regulation.

5 | CONCLUSION

TauCEST detection is feasible in the brain of polar cod at low temperatures. The majority of the total CEST effect observed in vivo is attributed to taurine (about 65%), with only small contributions from other amino acids (35%). TauCEST imaging provides non-invasive detection of relative changes in pH_i with high temporal and spatial resolution under acute exposure to high pCO_2. Future studies using this methodology may provide a new possibility to investigate the mechanisms underlying neurological and behavioural disorders of fish under OA scenarios and the associated influences of acid–base disturbances.

ORCID

Christian Bock 🆔 http://orcid.org/0000-0003-0052-3090

REFERENCES

1. Ward KM, Aletras AH, Balaban RS. A new class of contrast agents for MRI based on proton chemical exchange dependent saturation transfer (CEST). *J Magn Reson*. 2000;143(1):79-87.

2. Ward KM, Balaban RS. Determination of pH using water protons and chemical exchange dependent saturation transfer (CEST). *Magn Reson Med*. 2000;44(5):799-802.

3. Cai K, Haris M, Singh A, et al. Magnetic resonance imaging of glutamate. *Nat Med*. 2012;18(2):302-306.

4. Walker-Samuel S, Ramasawmy R, Torrealdea F, et al. In vivo imaging of glucose uptake and metabolism in tumors. *Nat Med*. 2013;19(8):1067-1072.

5. Wermter FC, Bock C, Dreher W. Investigating GluCEST and its specificity for pH mapping at low temperatures. *NMR Biomed*. 2015;28(11):1507-1517.

6. Lee JS, Xia D, Jerschow A, Regatte RR. In vitro study of endogenous CEST agents at 3 T and 7 T. *Contrast Media Mol Imaging*. 2016;11(1):4-14.

7. Forster RP, Goldstein L. Amino acids and cell regulation. *Yale J Biol Med*. 1979;52(6):497-515.

8. Ripps H, Shen W. Review: taurine: a 'very essential' amino acid. *Mol Vis*. 2012;18:2673-2686.

9. De Graaf RA. *Vivo NMR Spectroscopy: Principles and Techniques*. New York, NY: Wiley; 2013.

10. Tkáč I, Rao R, Georgieff MK, Gruetter R. Developmental and regional changes in the neurochemical profile of the rat brain determined by in vivo ^{1}H NMR spectroscopy. *Magn Reson Med*. 2003;50(1):24-32.

11. Puka M, Sundell K, Lazarewicz JW, Lehmann A. Species differences in cerebral taurine concentrations correlate with brain water content. *Brain Res*. 1991;548(1/2):267-272.

12. Forster RP, Hannafin JA, Goldstein L. Osmoregulatory role of amino acids in brain of the elasmobranch, *Raja erinacea*. *Comp Biochem Physiol A Physiol*. 1978;60(1):25-30.

13. Boyd TA, Cha CJ, Forster RP, Goldstein L. Free amino acids in tissues of the skate *Raja erinacea* and the stingray *Dasyatis sabina*: effects of environmental dilution. *J Exp Zool*. 1977;199(3):435-442.

14. Tkáč I, Oz G, Adriany G, Uğurbil K, Gruetter R. In vivo ^{1}H NMR spectroscopy of the human brain at high magnetic fields: metabolite quantification at 4T vs. 7T. Magn Reson Med. 2009;62(4):868-879.

15. Pfeuffer J, Tkáč I, Provencher SW, Gruetter R. Toward an in vivo neurochemical profile: quantification of 18 metabolites in short-echo-time ^{1}H NMR spectra of the rat brain. J Magn Reson. 1999;141(1):104-120.

16. Mlynárik V, Cudalbu C, Xin L, Gruetter R. ^{1}H NMR spectroscopy of rat brain in vivo at 14.1 Tesla: improvements in quantification of the neurochemical profile. J Magn Reson. 2008;194(2):163-168.

17. Hong ST, Balla DZ, Shajan G, Choi C, Uğurbil K, Pohmann R. Enhanced neurochemical profile of the rat brain using in vivo ^{1}H NMR spectroscopy at 16.4 T. Magn Reson Med. 2011;65(1):28-34.

18. Field CB, Barros VR, Dokken DJ, et al. Climate Change 2014: Impacts, Adaptation, and Vulnerability. Part A: Global and Sectorial Aspects. Working Group II Contribution to the Fifth Assessment Report of the Intergovernmental Panel on Climate Change. New York, NY: Cambridge University Press; 2014.

19. Gattuso JP, Magnan A, Billé R, et al. Contrasting futures for ocean and society from different anthropogenic CO_2 emissions scenarios. Science. 2015;349(6243):aac4722.

20. Pörtner HO, Peck L, Somero G. Thermal limits and adaptation in marine Antarctic ectotherms: an integrative view. Phil Trans R Soc Lond B. 2007;362(1488):2233-2258.

21. Claiborne JB, Edwards SL, Morrison-Shetlar AI. Acid-base regulation in fishes: cellular and molecular mechanisms. J Exp Zool. 2002;293(3):302-319.

22. Ishimatsu A, Hayashi M, Kikkawa T. Fishes in high-CO_2, acidified oceans. Mar Ecol Prog Ser. 2008;373:295-302.

23. Melzner F, Gutowska MA, Langenbuch M, et al. Physiological basis for high CO_2 tolerance in marine ectothermic animals: pre-adaptation through lifestyle and ontogeny? Biogeosciences. 2009;6:2313-2331.

24. Munday PL, McCormick MI, Nilsson GE. Impact of global warming and rising CO_2 levels on coral reef fishes: what hope for the future? J Exp Biol. 2012;215(Pt 22):3865-3873.

25. Heuer RM, Grosell M. Physiological impacts of elevated carbon dioxide and ocean acidification on fish. Am J Physiol Regul Integr Comp Physiol. 2014;307(9):R1061-R1084.

26. Munday PL, Dixson DL, Donelson JM, et al. Ocean acidification impairs olfactory discrimination and homing ability of a marine fish. Proc Natl Acad Sci U S A. 2009;106(6):1848-1852.

27. Dixson DL, Munday PL, Jones GP. Ocean acidification disrupts the innate ability of fish to detect predator olfactory cues. Ecol Lett. 2010;13(1):68-75.

28. Pörtner HO. Climate variations and the physiological basis of temperature dependent biogeography: systemic to molecular hierarchy of thermal tolerance in animals. Comp Biochem Physiol A Mol Integr Physiol. 2002;132(4):739-761.

29. Pörtner HO, Giomi F. Nothing in experimental biology makes sense except in the light of ecology and evolution—correspondence on J. Exp. Biol. 216, 2771-2782. J Exp Biol. 2013;216(Pt23):4494-4495.

30. Schmidt M, Gerlach G, Leo E, et al. Impact of ocean warming and acidification on the behaviour of two co-occurring gadid species, Boreogadus saida and Gadus morhua, from Svalbard. Mar Ecol Prog Ser. 2017;571:183-191.

31. Lee J, Taira T, Pihlaja P, Ransom BR, Kaila K. Effects of CO_2 on excitatory transmission apparently caused by changes in intracellular pH in the rat hippocampal slice. Brain Res. 1996;706(2):210-216.

32. Sinning A, Hübner CA. Minireview: pH and synaptic transmission. FEBS Lett. 2013;587(13):1923-1928.

33. Pörtner HO, Boutilier RG, Tang Y, Toews DP. Determination of intracellular pH and P_{CO_2} after metabolic inhibition by fluoride and nitrilotriacetic acid. Respir Physiol. 1990;81(2):255-273.

34. Moon RB, Richards JH. Determination of intracellular pH by ^{31}P magnetic resonance. J Biol Chem. 1973;248(20):7276-7278.

35. Roberts JKM, Wade-Jardetzky N, Jardetsky O. Intracellular pH measurements by phosphorus-31 nuclear magnetic resonance. Influence of factors other than pH on phosphorus-31 chemical shifts. Biochemistry. 1981;20(19):5389-5394.

36. Van der Linden A, Verhoye M, Pörtner HO, Bock C. The strengths of in vivo magnetic resonance imaging (MRI) to study environmental adaptational physiology in fish. Magn Reson Mater Phys Biol Med. 2004;17(3–6):236-248.

37. Bock C, Sartoris FJ, Pörtner HO. In vivo MR spectroscopy and MR imaging on non-anaesthetized marine fish: techniques and first results. Magn Reson Imaging. 2002;20(2):165-172.

38. Bock C, Lurman GJ, Wittig RM, Webber DM, Pörtner HO. Muscle bioenergetics of speeding fish: in vivo ^{31}P-NMR studies in a 4.7 T MR scanner with an integrated swim tunnel. Concepts Magn Reson Part B Magn Reson Eng. 2008;33B(1):62-73.

39. Gruetter R. Automatic, localized in vivo adjustment of all first- and second-order shim coils. Magn Reson Med. 1993;29(6):804-811.

40. Zaiss M, Schmitt B, Bachert P. Quantitative separation of CEST effect from magnetization transfer and spillover effects by Lorentzian-line-fit analysis of z-spectra. J Magn Reson. 2011;211(2):149-155.

41. Zong X, Wang P, Kim SG, Jin T. Sensitivity and source of amine-proton exchange and amide-proton transfer magnetic resonance imaging in cerebral ischemia. Magn Reson Med. 2013;71(1):118-132.

42. Sun PZ. Simplified and scalable numerical solution for describing multi-pool chemical exchange saturation transfer (CEST) MRI contrast. J Magn Reson. 2010;205(2):235-241.

43. Schmidt M, Windisch HS, Luwichowski KU, et al. Differences in neurochemical profiles of two gadid species under ocean warming and acidification. Front Zool. 2017;14:49.

44. Woessner DE, Zhang S, Merritt ME, Sherry AD. Numerical solution of the Bloch equations provides insights into the optimum design of PARACEST agents for MRI. Magn Reson Med. 2005;53(4):790-799.

45. Randtke EA, Chen LQ, Corrales RL, Pagel MD. The Hanes-Woolf linear QUESP method improves the measurements of fast chemical exchange rates with CEST MRI. Magn Reson Med. 2014;71(4):1603-1612.

46. Bottomley PA. Spatial localization in NMR spectroscopy in vivo. Ann N Y Acad Sci. 1987;508(1):333-348.

47. Tkáč I, Starcuk Z, Choi IY, Gruetter R. In vivo ^{1}H NMR spectroscopy of rat brain at 1 ms echo time. Magn Reson Med. 1999;41(4):649-656.

48. Eastman JT, Lannoo MJ. Diversification of brain morphology in Antarctic notothenioid fishes: basic descriptions and ecological considerations. *J Morphol*. 1995;223(1):47-83.

49. Woodward CK, Hilton BD. Hydrogen isotope exchange kinetics of single protons in bovine pancreatic trypsin inhibitor. *Biophys J*. 1980;32(1):561-575.

50. Eriksson MA, Härd T, Nilsson L. On the pH dependence of amide proton exchange rates in proteins. *Biophys J*. 1995;69(2):329-339.

51. Goerke S, Zaiss M, Bachert P. Characterization of creatine guanidinium proton exchange by water-exchange (WEX) spectroscopy for absolute-pH CEST imaging *in vitro*. *NMR Biomed*. 2014;27(5):507-518.

52. Sun PZ, van Zijl PC, Zhou J. Optimization of the irradiation power in chemical exchange dependent saturation transfer experiments. *J Magn Reson*. 2005;175(2):193-200.

53. Haris M, Cai K, Singh A, Hariharan H, Reddy R. *In vivo* mapping of brain myo-inositol. *Neuroimage*. 2011;54(3):2079-2085.

54. Haris M, Nanga RP, Singh A, et al. Exchange rates of creatine kinase metabolites: feasibility of imaging creatine by chemical exchange saturation transfer MRI. *NMR Biomed*. 2012;25(11):1305-1309.

55. Nagarajan R, Ramadan S, Thomas MA. Detection of amide and aromatic proton resonances of human brain metabolites using localized correlated spectroscopy combined with two different water suppression schemes. *Magn Reson Insights*. 2010;2010(4):1-9.

56. Sugita N. Comparative studies on the growth of the cerebral cortex. I. On the changes in the size and shape of the cerebrum during the postnatal growth of the brain. Albino rat. *J Comp Neurol*. 1917;28(3):495-510.

57. Kabli S, Spaink HP, De Groot HJ, Alia A. *In vivo* metabolite profile of adult zebrafish brain obtained by high-resolution localized magnetic resonance spectroscopy. *J Magn Reson Imaging*. 2009;29(2):275-281.

58. Ishimatsu A, Kikkawa T, Hayashi M, Lee KS, Kita J. Effects of CO_2 on marine fish: larvae and adults. *J Oceanogr*. 2004;60(4):731-741.

59. Hylland P, Nilsson GE. Extracellular levels of amino acid neurotransmitters during anoxia and forced energy deficiency in crucian carp brain. *Brain Res*. 1999;823(1/2):49-58.

60. Franks NP, Lieb WR. Molecular and cellular mechanisms of general anaesthesia. *Nature*. 1994;367(6464):607-614.

61. Iwama GK, McGeer JC, Pawluk MP. The effects of five fish anaesthetics on acid-base balance, hematocrit, blood gases, cortisol, and adrenaline in rainbow trout. *Can J Zool*. 1989;67(8):2065-2073.

62. Wittmann AC, Pörtner HO. Sensitivities of extant animal taxa to ocean acidification. *Nat Clim Chang*. 2013;3:995-1001.

63. Larsen BK, Pörtner HO, Jensen FB. Extra- and intracellular acid-base balance and ionic regulation in cod (*Gadus morhua*) during combined and isolated exposures to hypercapnia and copper. *Mar Biol*. 1997;128(2):337-346.

64. Tkáč I, Henry PG, Zacharoff L, et al. Homeostatic adaptations in brain energy metabolism in mouse models of Huntington disease. *J Cereb Blood Flow Metab*. 2012;32(11):1977-1988.

65. Deelchand DK, Nguyen TM, Zhu XH, Mochel F, Henry PG. Quantification of *in vivo* ^{31}P NMR brain spectra using LCModel. *NMR Biomed*. 2015;28(6):633-641.

66. Haris M, Nath K, Cai K, et al. Imaging of glutamate neurotransmitter alterations in Alzheimer's disease. *NMR Biomed*. 2013;26(4):386-391.

67. Singh A, Cai K, Haris M, Hariharan H, Reddy R. On B_1 inhomogeneity correction of *in vivo* human brain glutamate chemical exchange saturation transfer contrast at 7T. *Magn Reson Med*. 2013;69(3):818-824.

68. Kogan F, Singh A, Debrosse C, et al. Imaging of glutamate in the spinal cord using GluCEST. *Neuroimage*. 2013;77:262-267.

69. Henkelman RM, Stanisz GJ, Graham SJ. Magnetization transfer in MRI: a review. *NMR Biomed*. 2001;14(2):57-64.

70. Leibfritz D, Dreher W. Magnetization transfer MRS. *NMR Biomed*. 2001;14(2):65-76.

SUPPORTING INFORMATION

Additional supporting information may be found online in the Supporting Information section at the end of the article.